Auditory deviants evoke cortical state changes under anesthesia

Laura H Bohórquez[1,2,3], Manuel S Malmierca[1,2,3,*], Adam Hockley[1,2,3,4,**]

[1] Cognitive and Auditory Neuroscience Laboratory, Institute of Neuroscience of Castilla y León (INCYL), Salamanca, Spain
2 Salamanca Institute for Biomedical Research (IBSAL), Salamanca, Spain
3 Department of Cell Biology and Pathology, Faculty of Medicine, University of Salamanca, Salamanca, Spain
4 Lead contact
* Correspondence msm@usal.es
** Correspondence adamhockley@gmail.com

SUMMARY

Context-dependent sensory processing within the predictive coding framework relies on detecting mismatches between incoming stimuli and internal predictive models. Sensory deviants elicit prediction errors, seen as enhanced neural responses, that update these models and influence attention and behavior. Although prediction errors have been widely observed across the brain, the downstream processes that link them to attentional shifts and decision-making remain poorly understood. In this study, we recorded electrocorticography in urethane-anesthetized rats and identified robust cortical slow oscillations, characterized by reliable transitions between “Up” and “Down” states. Deviant stimuli in an auditory oddball paradigm evoked an initial prediction error, followed by prolonged, all-or-nothing cortical Up states whose occurrence depended on anesthetic depth. These results indicate that, under anesthesia, sensory deviants trigger cortical state transitions, suggesting that in wakefulness, such shifts may support attentional reorientation and behavioral decision-making.

KEYWORDS

Mismatch negativity, Up state, cortical slow oscillations, synchronized activity, anesthesia, auditory cortex, prefrontal cortex, omission, prediction error, P300

INTRODUCTION

Context modulates neural processing of sensory stimuli. The brain suppresses responses to predictable inputs and amplifies responses to unexpected ones. This deviance detection mechanism enhances the salience of unpredictable events that often carry survival-relevant information. Predictive coding provides a framework for understanding contextual processing, wherein the brain (1) encodes regular patterns to form internal predictive models, (2) detects deviations from those models, and (3) updates the models to guide attention and behavioral choices. Extensive work has characterized prediction error responses to deviant auditory stimuli across a range of paradigms [1–5]. However, the mechanisms by which prediction errors influence attention and behavior remain less well understood. In monkeys, auditory cortex neurons generate early (~100 ms) and late (~300 ms) responses to deviant stimuli during attention-demanding task [6], The early response coincides with the mismatch negativity (MMN), while the late response correlates with behavioral decisions. Cortical state changes accompany attention and behavioral choice [7–9], and prediction errors can induce cognitive state transitions between behavioral tasks [10]. Because cortical state changes support attentive decision-making [9,11–13], prediction errors may initiate these transitions to direct attention and shape behavioral responses.

Cortical slow oscillations exemplify cortical state changes and emerge during the synchronized brain states of slow-wave sleep and anesthesia. These oscillations occur globally across the cortex, thalamus, and hippocampus, and involve reliable transitions between “Up” states of high neural activity and “Down” states of low activity [14–17]. During slow-wave sleep and deep anesthesia, the brain generates Up/Down transitions at a frequency of 0.2–0.5 Hz [18]. Studies using methods ranging from in vitro single-cell recordings to scalp electroencephalography consistently record slow oscillations [19,20].

Thalamic input plays a critical role in initiating cortical Up states. Although the cortex continues to generate slow oscillations after deafferentation [21], inactivating the thalamus markedly reduces their frequency [22–24]. Thalamocortical activity consistently precedes the onset of Up states, indicating that this input likely initiates the transitions and regulates their frequency [25]. External somatosensory and visual stimuli also trigger cortical Up states, with each wave originating in the corresponding sensory region [26–28]. Based on this evidence, we propose the hypothesis that deviant stimuli in the oddball paradigm may increase thalamocortical drive and thereby evoke Up states.

We selected urethane anesthesia to model cortical state transitions because it induces the full spectrum of the sleep cycle, including regular, rhythmic alternations between Up and Down states [29–35]. We recorded electrocorticography (ECoG) signals under urethane and observed spontaneous Up states during silent periods. Unexpected stimuli in the oddball paradigm consistently evoked Up states. The binary nature of Up state triggering generated bimodal amplitude distributions, and the resulting all-or-nothing, long-latency responses matched the profile of cortical slow oscillations. Deviant stimuli in auditory cortex elicited an initial peak at 50 ms and 20 μV, followed by a later peak at 200 ms and 200 μV, and these responses propagated across cortical areas as traveling Up state waves. The timing of preceding Up states constrained the likelihood of new ones, consistent with a refractory period. Anesthetic depth shaped the brain’s responsiveness to deviant stimuli, determining whether they triggered an Up state.

RESULTS

Urethane anesthesia induces spontaneous Up and Down states

We surgically implanted ECoG arrays in five rats, placing electrodes over left and right auditory cortex (AC-L and AC-R) and medial prefrontal cortex (mPFC-L and mPFC-R) (Fig. 1A), and began recordings 4–6 hours after anesthetic induction. In the absence of sensory stimulation, we observed spontaneous Up states occurring simultaneously across all six electrodes at a frequency of approximately 0.2 Hz in filtered (1–150 Hz) local field potentials (LFPs; Fig. 1B). These Up states featured increased activity lasting 1–3 seconds across traditional oscillatory bands, with high-frequency activity nested within the Up state (Fig. 1C–E). These findings confirm that urethane anesthesia actively generates spontaneous Up and Down state dynamics.

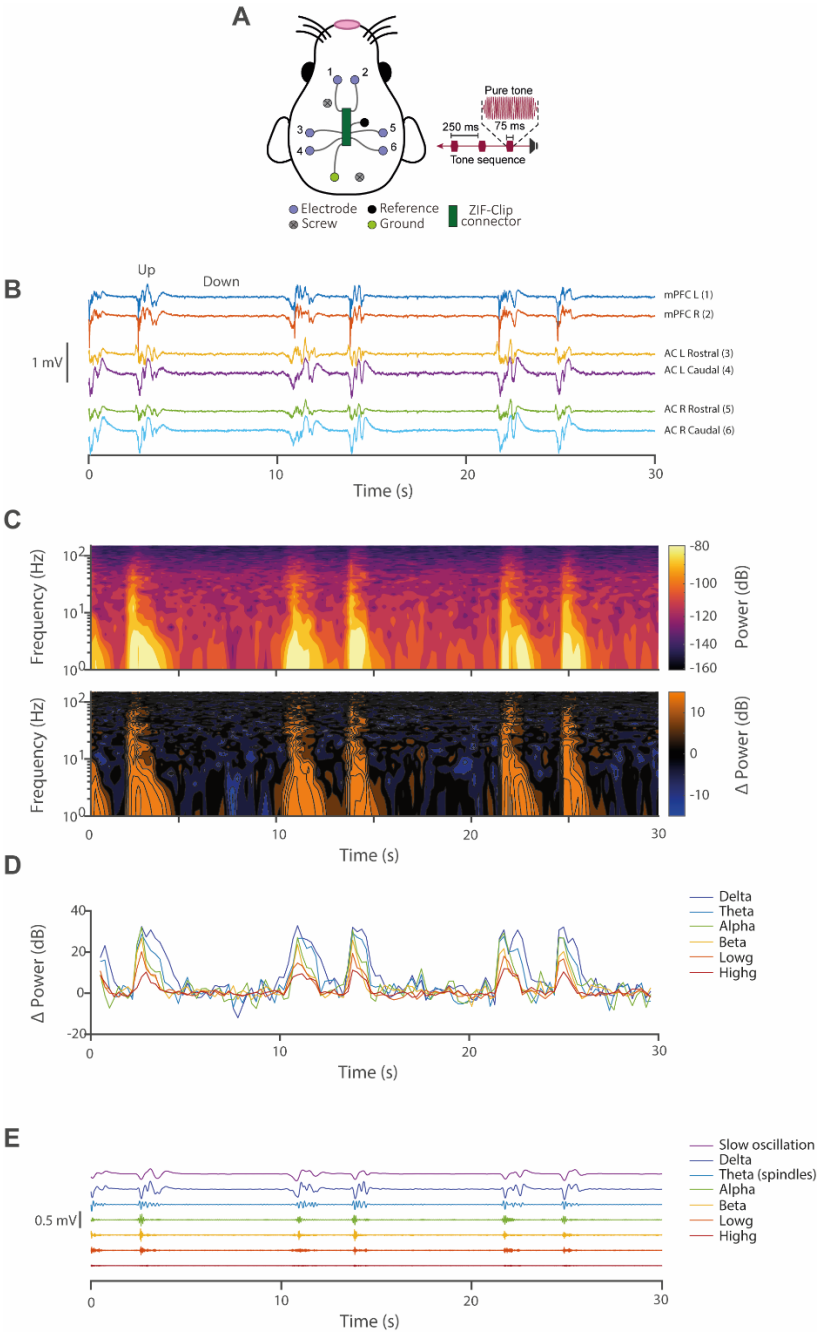

Figure 1: Spontaneous Up and Down states in the urethane-anesthetised rat. A) Schematic of the six recording sites, two over mPFC (1 & 2) and four over AC, bilaterally placed with rostral (3 & 5) and caudal sites (4 & 6). **B)** Example simultaneous LFP traces from all six electrode sites show that Up states are coincidental across electrode sites. Data from 30s of silence is shown, during which cortical Up and Down states are observed. **C)** Spontaneous cortical Up states are associated with increased activity across oscillatory bands. Top shows spontaneous power for the LFP trace in B. Spontaneous increases occur across traditional oscillators bands and align with LFP trace peaks. Bottom shows change in power from baseline. **D)** Oscillatory power traces demonstrate coincidental increases across all power bands. **E)** Low- and high-frequency components of the LFP are shown by filtering for specific frequency bands.

Auditory deviants evoke cortical Up states

To determine whether the auditory oddball paradigm evokes cortical Up states, we presented a repeating standard (STD) tone of 10 kHz interspersed with rare deviant (DEV) tones of 14.142 kHz (75 ms duration, 250 ms stimulus onset asynchrony (SOA), 6.45% DEV probability, inter-DEV interval 3–4.75 s, 60 dB SPL) while recording ECoG activity as shown in Fig. 1. The inter-DEV interval produced a deviant presentation rate of approximately 0.2–0.35 Hz, which varied randomly but matched the spontaneous Up state frequency. Up states can be identified in LFPs [30,36] thus following previous methods using LFPs we identified Up state initiations as the first negative peaks in the filtered (0.1–10 Hz) LFP traces from the mPFC-L electrode (Fig. 2A, black dots). We selected mPFC-L for Up state detection due to its superior signal-to-noise ratio, although Up states appeared simultaneously across all electrode sites, as shown in Fig. 1B.

In all animals, a high proportion of DEV stimuli triggered cortical Up states (M = 57%, SD = 20.1). These responses frequently lasted 1–3 seconds, indicating sustained changes in cortical activity. To quantify the reliability of this effect, we measured the temporal relationship between stimulus onset and Up state initiation using cross-correlation synchrony (Fig. 2B). We compared DEV-Up synchrony to the synchrony between Up states and the STD tones that occurred 2–5 trials before each deviant. Across animals, DEV stimuli consistently evoked Up states, with DEV-Up synchrony significantly exceeding STD-Up synchrony and peaking around 200 ms after stimulus onset (Fig. 2E).

To test whether deviant responses followed a bimodal distribution, consistent with the all-or-nothing nature of Up state initiation, we calculated the root-mean-square (RMS) amplitude from 0 to 500 ms following each DEV and plotted the distribution. This analysis revealed a clear bimodal response profile in both the example animal (Fig. 2C) and in the group average after normalizing RMS values within each animal (Fig. 2F). We then separated the deviant responses by the presence or absence of an Up state initiation. When an Up state occurred, the signal exhibited a negative peak at approximately 200 ms, followed by a long-latency component that extended up to 850 ms (example trace in Fig. 2D, group average in Fig. 2G).

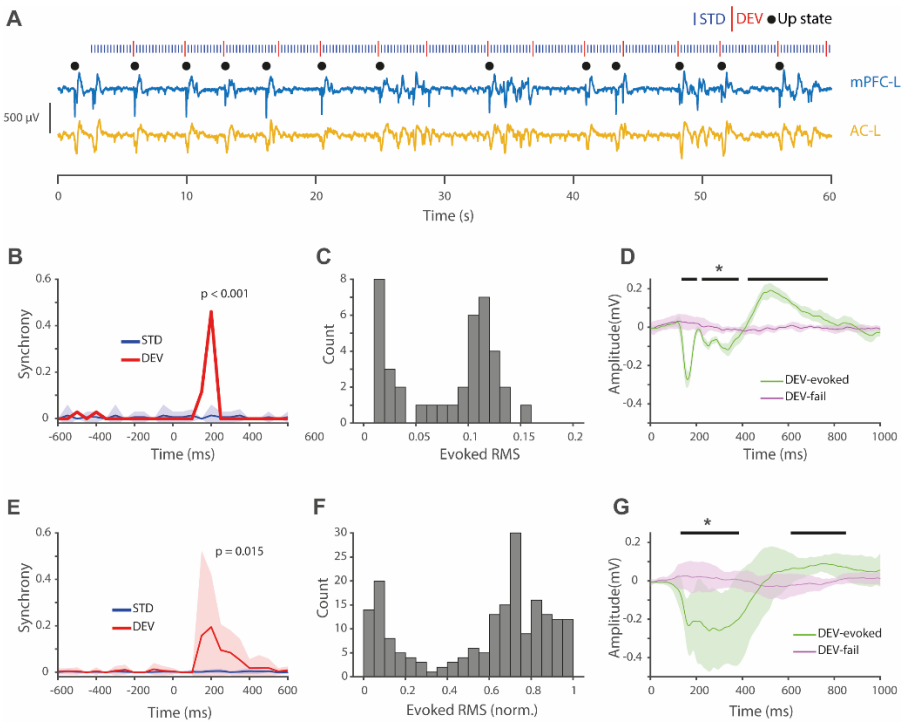

Figure 2: Auditory deviants initiate Up states in the mPFC. A) LFP traces from the mPFC-L (blue) and AC-L (yellow), electrode sites 1 and 3, respectively from an example animal. An auditory oddball paradigm was presented with a SOA of 250 ms and inter-DEV interval of 3 - 4.75 s (11 – 18 STDs (blue bars; pseudorandomised). Auditory DEV (red bar) was often followed by Up state initiation (black dot). For clarity only the initial 30s are shown, full stimuli length was 620 stimuli, 40 DEVs, 155s. **B)** Cross-correlation synchrony between Up state initiation and DEV or STD stimuli presentation for the example animal in panel A. Significantly higher synchrony in the DEV condition compared to the STD (Mean ± 95% CI for the STDs 2-5 stimuli before a DEV) condition is observed with a ~200ms latency, demonstrating reliable initiation of cortical Up state by the auditory DEV. Two-sample t-test used for statistical comparison. **C)** Histogram of evoked RMS in the 0-500ms window following DEV stimuli, for the example animal in panel A. Response RMS to DEV stimuli is bimodal, indicating an all-or-nothing response, not a simple auditory response. **D)** For the example animal in panel A, we partitioned mPFC LFP responses to DEV stimuli by whether an Up state is initiated. When DEVs evoked an Up state (green), a negative peak occurred at ~200 ms then a long-latency response up to 850 ms in duration. In comparison, when DEVs failed to evoke an Up state (purple), no other response is observed. Black bar mark significance between DEV-evoked and DEV-fail (two-sample t-test, α=0.05). 0ms represents the DEV stimulus onset. **E-G)** The same analyses as panels B-D but average data across all animals (n=6).

We next tested a classical oddball paradigm with a 500 ms SOA, 10% DEV probability, and a mean inter-DEV interval of 5 s, using a flip-flop design with 10 and 14.142 kHz tones (75 ms duration, 60 dB SPL; Fig. 3A). As in Fig. 2, we observed spontaneous and deviant-evoked responses that followed an all-or-nothing, long-latency profile. To investigate sites of Up state initiation and propagation, we compared deviant responses across AC-L, AC-R, and mPFC-L. When a deviant triggered an Up state, response amplitudes exceeded those observed during non-evoked trials (Fig. 3B,E). The AC-L showed the shortest latency response to deviants (45.87 ms), followed by later responses in AC-R (186.11 ms) and mPFC-L (263.43 ms).

We then compared responses to DEV and STD stimuli of different frequencies in AC-L (Fig. 3C,F) to assess whether standard tones could also evoke Up states. Because cortical neurons must recover from synaptic adaptation following an Up state [37], we tested whether the time since the previous Up state influenced the probability of Up state initiation. Deviants that failed to evoke an Up state followed more

closely after a prior Up state, consistent with a refractory period (Fig. 3D,G). In contrast, these non-evoking deviants did not occur sooner after the previous deviant, indicating that stimulus timing alone did not explain the failure to initiate an Up state.

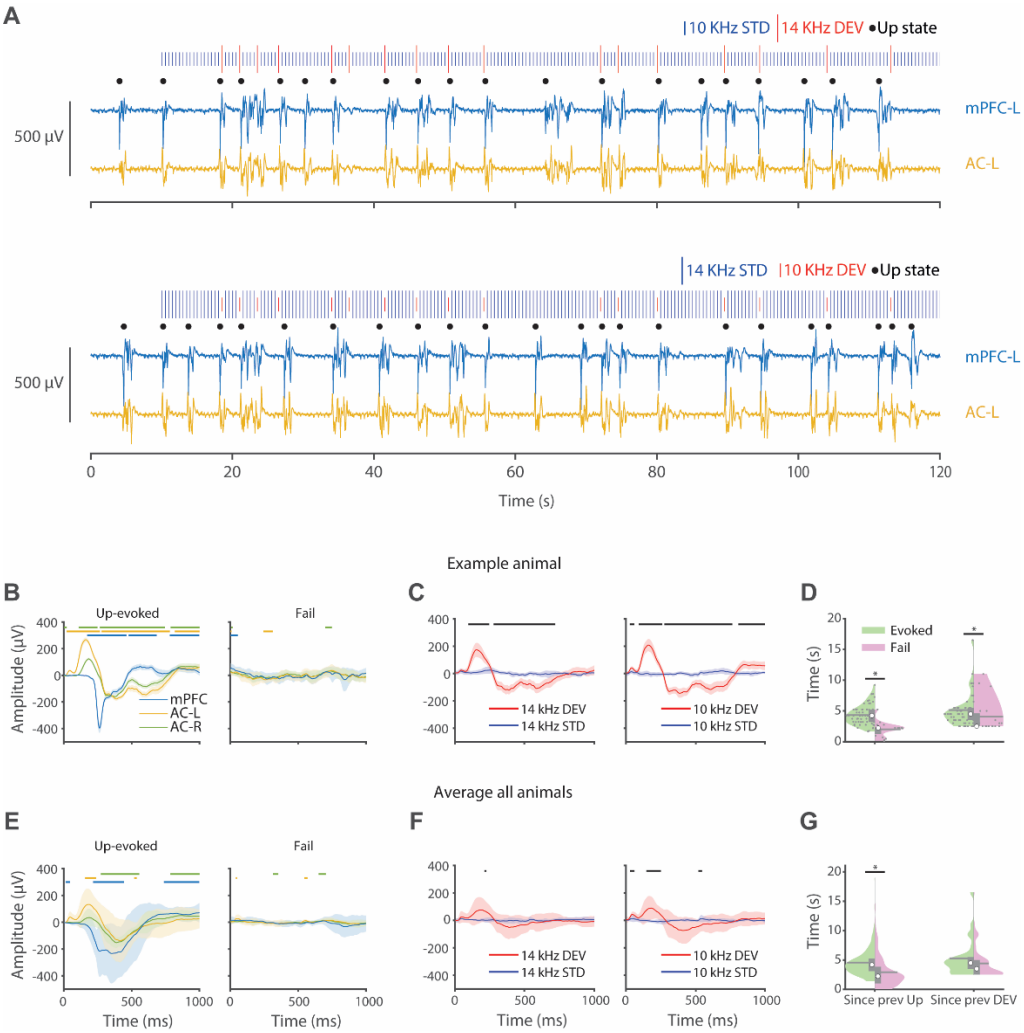

Figure 3: A generic auditory Oddball paradigm also initiates cortical Up states. A) LFP traces from mPFC-L (blue) and AC-L (yellow) electrodes for an example animal. For each animal, a classical oddball paradigm was presented with a 500 ms SOA and 10% DEV probability. Stimuli length was 75 ms, 10% DEV probability, 82 minutes. **B)** Plots of DEV response from an example animal at different electrodes sites when the DEV is followed by an Up state (left) or not followed by an Up state (right). Green, yellow and blue bars indicate the presence of significance from 0 for AC-R, AC-L and mPFC-L, respectively (one sample t-test, $p<0.05$). **C)** Comparison of LFP responses to DEV and STD stimuli of 14 kHz (left) and 10kHz (right) in the AC-L from an example animal. Black bar indicates the significance (two sample unpaired t-test, $p<0.05$). **D)** Effect of the time elapsed between the previous DEV or the previous Up state on subsequent Up state evocation. Violin plots from an example animal show trials which evoked (green) or failed to evoke (pink) Up states, and the time since a previous Up state (left) or since previous DEV (right) (* $p<0.05$, Wilcoxon test,). **E, F, G:** As in B, C, D but average data across all animals.

Anesthetic depth modulates deviant-evoked cortical Up states

To determine whether anesthesia is necessary for deviant-evoked Up states, we chronically implanted an ECoG array in one rat and recorded activity 11 weeks post-implant. We compared responses in the

awake state and under urethane anesthesia in the same animal, using identical auditory stimuli one hour after anesthetic induction. At this point, the animal reached a surgical level of anesthesia and showed areflexia. We presented a flip-flop oddball paradigm (75 ms duration, 250 ms SOA; 10% DEV probability; mean inter-DEV interval 2.5 s; 10/14.142 kHz tones at 75 dB SPL;). During wakefulness, LFP traces showed smaller amplitudes (Fig. 4), indicating a desynchronized state. One hour after urethane administration, the brain entered a synchronized state with clear cortical slow oscillations (Fig. 4A). In both the PFC-L (Fig. 4B) and AC-L (Fig. 4C), deviant stimuli evoked stronger long-latency responses under anesthesia than in the awake state, consistent with cortical Up states.

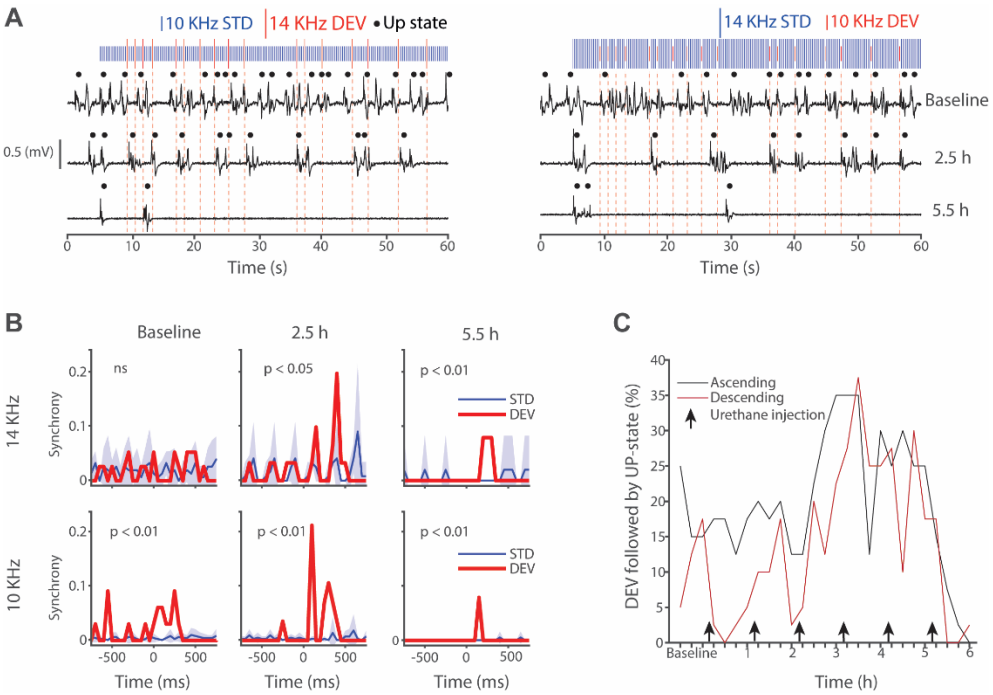

Figure 4. Up states occur only under anaesthesia. A) We compared DEV responses in awake and under anesthesia to study the presence of Up states. LFP trace examples are from awake and 1 hour after urethane injection. A flip-flop oddball paradigm was presented with a 250 SOA and 10% DEV probability. Stimuli length was 1600, 480 DEV, 43 minutes. **B**) LFP plot from mPFC-L for DEVs of 14 KHz (left) and 10 KHz (right), black line represents the awake recording and red the anesthetized one. On x axis 0 represents the DEV onset. Black bars show significance (two sample unpaired t-test, $p<0.05$). **C)** The same as E but for data from the AC-L.

To assess how anesthetic depth modulates long-latency deviant responses, we administered incremental doses of urethane to one rat. We presented a classical oddball paradigm (same parameters as above) and used a fixed 0.1 mV threshold to identify Up states across time. We began recording 6 hours after initial induction (baseline) and repeated stimulus presentations every 15 minutes over a 6-hour period while administering supplemental urethane. LFP traces from 14 kHz and 10 kHz deviants (Fig. 5A) showed a progressive decrease in Up state frequency with increasing anesthetic depth. Synchrony between deviant onset and Up state initiation increased with each urethane dose until very deep anesthesia reduced the likelihood of exiting Down states (Fig. 5B). We then calculated the percentage of deviants that evoked an Up state, which increased in parallel with synchrony as urethane levels rose (Fig. 5C). These findings indicate that both the presence and depth of anesthesia strongly influence the probability and timing of deviant-evoked Up states.

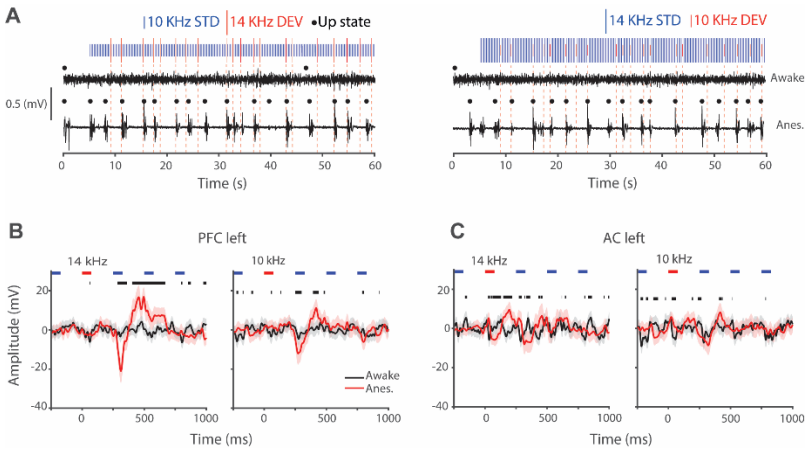

Figure 5: Deviants evoking cortical Up states is dependent on anaesthetic depth. A) In one animal, we gave supplemental urethane anesthetic doses to assess the impact on Up state initiations. LFP traces from baseline, is 6 hours after initial urethane induction; 2.5 and 5.5 hours after 5 and 8 supplementary urethane dosages; for an example animal. A classic oddball paradigm was presented with a 250 SOA and 10% DEV probability, to allow presentation every 15 minutes. Data shown are the initial 60 seconds, for clarity. Stimuli length was 75 ms, 40 DEV, 11 minutes. **B)** Cross-correlation synchrony between Up state initiation and DEV or STD stimuli for ascending or descending oddballs (top row & bottom row, respectively) (two sample unpaired t-test, *p<0.05). **C)** Percentage of DEV that are followed by Up states, throughout further urethane administration, for ascending or descending oddballs (black & red, respectively).

DISCUSSION

Our ECoG recordings in rats revealed spontaneously occurring Up and Down states under urethane anesthesia. When we presented an auditory oddball paradigm, only DEV stimuli evoked all-or-nothing long-latency responses that closely resembled features of cortical slow oscillation Up states. These deviant-evoked responses emerged first in AC at the shortest latency and then spread to other regions, consistent with the traveling wave dynamics of Up state propagation [38]. Deviants triggered Up states more reliably when a longer period had elapsed since the previous Up state, consistent with a refractory period. Critically, only anesthesia enabled deviant-evoked Up states, and the effect scaled with anesthetic depth. STD stimuli failed to initiate Up states. When deviants did not trigger an Up state, we observed minimal deviant-related activity, suggesting that Up state initiation represents the principal cortical response to auditory deviance under urethane anesthesia (Fig. 3). These responses featured an early negative peak around 50 ms and 20 µV, consistent with the rat MMN [39], followed by a later, larger peak at 200 ms and 200 µV that we interpret as reflecting Up state initiation, given its absence during wakefulness.

Although our study does not directly address the mechanism by which deviants evoke Up states, previous work has shown that both thalamocortical activity [22–25] and sensory stimuli [26–28] can trigger Up states. Neurons in the auditory thalamus exhibit stimulus-specific adaptation and respond strongly to deviant stimuli [1,40,41]. Based on this, we suggest that enhanced deviant responses in the auditory thalamus during the oddball paradigm increase thalamocortical drive and thereby evoke cortical Up states. Our findings support this interpretation, as Up states appear to initiate in the AC-L, the primary site of thalamocortical input during right-ear stimulus presentation. These Up states then propagate across the cortex as traveling waves at an estimated rate of ~30 mm/s [42,43], which likely accounts for the delayed responses observed in AC-R and mPFC-L (Fig. 3B,E). Future studies using this same paradigm while selectively inhibiting thalamocortical input could confirm this proposed mechanism.

If the mechanism we suggest is correct, adaptive and predictive processes that shape thalamocortical activity may play a central role in generating sensory cortex responses to deviants during unconscious

233 states. Thalamocortical input would evoke cortical Up states from the primary sensory cortex and
234 propagate them across the cortex as traveling waves [20,38,44]. An enhanced thalamic response to deviant
235 (but not standard) stimuli could therefore generate a long-latency mismatch response throughout the
236 cortex. Although such responses may reflect stimulus-specific adaptation or prediction error within the
237 thalamus, they may not represent true prediction error signals in all cortical areas. Instead, these
238 responses may arise solely from increased thalamocortical drive sufficient to initiate an Up state. Future
239 studies that record cortical Up states while manipulating thalamocortical pathways could evaluate this
240 potential mechanism. If this account holds, interpreting long-latency prediction error signals in the cortex
241 during unconscious states requires caution.

242 We conducted a test to examine whether omitted stimuli could evoke cortical Up states, using two
243 omission paradigms with different SOAs. In one condition (Rats 3 and 4), we used a 250 ms SOA (75 ms
244 duration 6.45% omission probability; inter-omission interval 3–4.75 s; STD 10 kHz, 60 dB SPL), and in the
245 other (Rats 5 and 6), we used a 125 ms SOA (6.45% omission probability; inter-omission interval 1.5–
246 2.375 s; same tone parameters). In both cases, we observed no evidence that omissions alone initiated
247 cortical Up states (Fig. 6). However, in the 250 ms SOA condition, the post-omission stimuli frequently
248 evoked Up states, and the timing of these responses corresponded more closely with the onset of the
249 post-omitted tone than with the omission itself (two-sample t-test, $p = 0.0019$). These findings remain
250 preliminary, and future experiments with larger samples and optimized paradigms will be necessary to
251 clarify whether omissions can modulate Up state dynamics under anesthesia. Omissions induce negative
252 prediction errors, which are present in a lower number of neurons and at lower activity rates than positive
253 prediction errors or responses to standard stimuli [45–50]. Negative prediction errors would therefore be
254 unlikely to increase cortical activity sufficiently to evoke Up states.

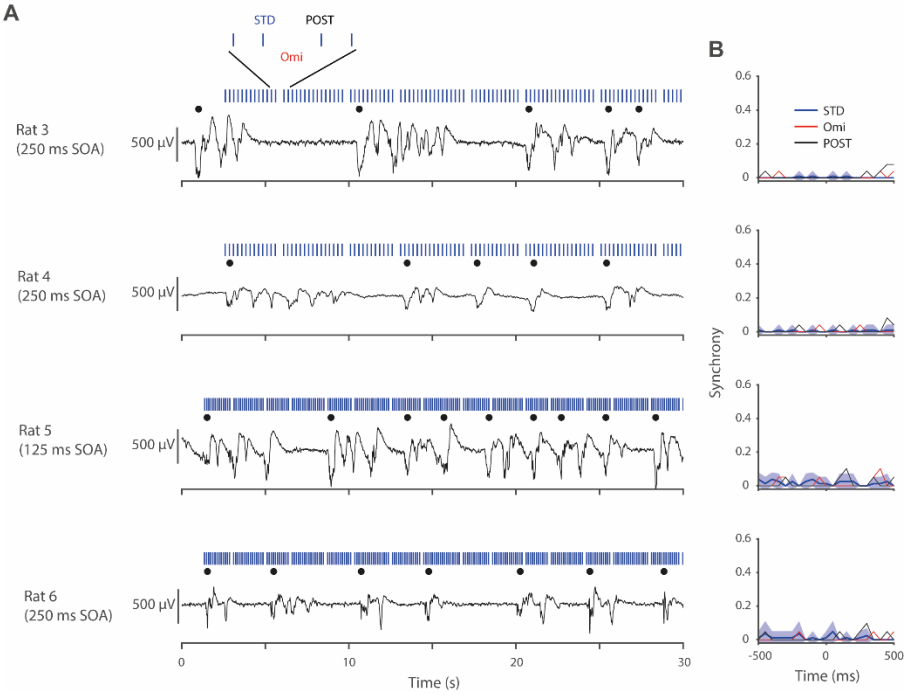

255

256 **Figure 6: Omissions do not evoke cortical Up states. A)** LFP traces from the mPFC-L. We tested in
257 animals 3-6 (rows), omission paradigms consisting of a repeating STD (blue bars) and omission (spaces)
258 for Up state initiation (black dots). We tested animals 3&4 with a 250 ms SOA, and animals 5&6 with a
259 125 ms SOA. For clarity only the initial 30s are shown, full stimuli length was 620 stimuli, 40 DEVs,
260 77/155s. **B)** Cross-correlation synchrony between Up state initiation and omission or STD stimuli
261 presentation revealed that silent omission or repeating STD stimuli did not initiate cortical Up states in any
262 animal. However, the post-omission stimuli were able to evoke Up states in the 250 ms SOA condition in
263 Rats 3 & 4 (two-sample t-test, p = 0.0019). The latency of Up state evoking is consistent with Up state
264 evoking by the post-omission.

Previous studies have described long-latency cortical responses to auditory deviants during anesthesia and synchronized sleep, but have not linked these responses to cortical state changes [1,51–56]. Based on our present data, we suggest that long-latency deviant responses may reflect a state change within the desynchronized brain state of deep anesthesia, which resembles non-rapid eye movement (NREM) sleep [8]. MMN is a sensory-evoked potential that serves as a biomarker for numerous neuropsychological disorders [57–60], although debate continues regarding its underlying neural mechanisms [61–64]. Studies have observed MMN and related neural activity during sleep [65–67] and under anesthesia [68–71], and some have reported that neuronal correlates of MMN, such as stimulus-specific adaptation, can even increase in certain anesthetic states [72,73].

Our data show a typical rat MMN response at ~50 ms in primary auditory cortex [39], followed by a long-latency response at ~200 ms that occurs exclusively in response to deviant stimuli. We attribute this later response to the initiation of cortical Up states, as it matches spontaneous Up states in waveform, occurs in an all-or-nothing fashion, propagates globally across the cortex as a traveling wave, and varies with anesthetic depth. This long-latency activity may resemble the human P300 component of the event-related potential, which reflects novelty detection, context updating, and higher-order cognitive processing [74–76].

By administering supplemental doses of urethane, we demonstrated that the ability of deviants to trigger Up states depends on anesthetic depth (Fig. 5). When we compared this to recordings from an awake animal, we found that Up state responses did not occur globally during wakefulness (Fig. 4). Anesthetic depth influences the duration of Up and Down states, with deeper anesthesia increasing the time spent in the Down state [35]. At low urethane doses, some studies report increased cortical complexity [36,77], while others show that animals spend more time in NREM-like states than in REM-like states [35]. In our data, animals in a more synchronized state (characterized by robust and rhythmic Up and Down states) showed more consistent Up state initiation in response to deviants (Fig. 5). This dependence on anesthetic depth likely reflects the increased difficulty of transitioning out of the Down state under deeper anesthesia [35].

The long-latency deviant response observed in our data appears to result solely from a state change during the desynchronized brain state of deep anesthesia, which resembles NREM sleep. However, its relationship to processing in the awake brain remains unknown. We did not observe any long-latency state changes during wakefulness, which may reflect the more subtle and localized cortical state dynamics typical of wakefulness, or the passive nature of our awake recordings, which lacked directed attention to the deviant [7,8]. Because this response follows the traditional MMN, it may more closely resemble the P300 [74–76] or the late deviant responses associated with behavioral decisions [6]. Previous studies show that unexpected stimuli can induce cognitive state transitions between behavioral tasks [10] and influence behavior through underlying neural changes [78,79]. The cortical state changes we describe here could support MMN models that emphasize shifts in attention [80,81]. A global cortical state change driven by unexpected stimuli, accompanied by traveling wave propagation, may also explain the modality-independent surprise-evoked potentials reported in other studies [82].

RESOURCE AVAILABILITY

Lead contact

Further information and requests for resources and reagents should be directed to and will be fulfilled by the lead contact, Adam Hockley (dradamhockley@gmail.com).

Materials availability

No new reagents or materials were generated for this study.

Data and code availability

- All data will be deposited at Zenodo at 10.5281/zenodo.15791248
- Analysis code will be deposited at Zenodo at 10.5281/zenodo.15791285
- Any additional information required to reanalyse the data reported in this paper is available from the lead contact upon request.

ACKNOWLEDGMENTS

This study was supported by projects PROOPI340-USAL4EXCELLENCE funded by H2020-MSCA-COFUND-2020 to AH and MSM; PID2023-148541OB-I00 funded by MCIN/AEI to MSM; Foundation Ramón Areces grant CIVP20A6616 to MSM; and Consejería de Educación, Junta de Castilla y León (SA218P23) to MSM. LHB was supported by a fellowship from the AEI PREP2023-148541OB funded by MCIN/AEI/10.13039/501100011033 and FSE

AUTHOR CONTRIBUTIONS

Laura H Bohorquez: Methodology, Software, Formal analysis, Investigation, Writing - Original Draft, Writing – Review & Editing, Visualization

Manuel S Malmierca: Conceptualization, Writing – Review & Editing, Supervision, Funding acquisition

Adam Hockley: Conceptualization, Methodology, Software, Formal analysis, Investigation, Writing - Original Draft, Writing – Review & Editing, Visualization, Supervision, Funding acquisition

DECLARATION OF INTERESTS

The authors declare no competing interests.

SUPPLEMENTAL INFORMATION

REFERENCES

1. Parras, G.G., Nieto-Diego, J., Carbajal, G. V., Valdés-Baizabal, C., Escera, C., and Malmierca, M.S. (2017). Neurons along the auditory pathway exhibit a hierarchical organization of prediction error. Nat. Commun. *8*. https://doi.org/10.1038/s41467-017-02038-6.

2. Shymkiv, Y., Hamm, J.P., Escola, S., and Yuste, R. (2025). Slow cortical dynamics generate context processing and novelty detection. Neuron, 1–11. https://doi.org/10.1016/j.neuron.2025.01.011.

3. Audette, N.J., Zhou, W.X., La Chioma, A., and Schneider, D.M. (2022). Precise movement-based predictions in the mouse auditory cortex. Curr. Biol. *32*, 4925-4940.e6. https://doi.org/10.1016/j.cub.2022.09.064.

4. Gelens, F., Äijälä, J., Komatsu, M., Uran, C., Jensen, M.A., Miller, K.J., Ince, R.A.A., Vinck, M., and Canales-Johnson, A. (2024). Distributed representations of prediction error signals across the cortical hierarchy are synergistic. Nat. Commun. *2024*. https://doi.org/10.1038/s41467-024-48329-7.

5. Dürschmid, S., Edwards, E., Reichert, C., Dewar, C., Hinrichs, H., Heinze, H.J., Kirsch, H.E., Dalal, S.S., Deouell, L.Y., and Knight, R.T. (2016). Hierarchy of prediction errors for auditory events in human temporal and frontal cortex. Proc. Natl. Acad. Sci. U. S. A. *113*, 6755–6760. https://doi.org/10.1073/pnas.1525030113.

6. Gong, Y., Song, P., Du, X., Zhai, Y., Xu, H., Ye, H., Bao, X., Huang, Q., Tu, Z., Chen, P., et al. (2024). Neural correlates of novelty detection in the primary auditory cortex of behaving monkeys. Cell Rep. *43*. https://doi.org/10.1016/j.celrep.2024.113864.

7. Speed, A., Del Rosario, J., Burgess, C.P., and Haider, B. (2019). Cortical State Fluctuations across Layers of V1 during Visual Spatial Perception. Cell Rep. *26*, 2868-2874.e3. https://doi.org/10.1016/j.celrep.2019.02.045.

8. Harris, K.D., and Thiele, A. (2011). Cortical state and attention. Nat. Rev. Neurosci. *12*, 509–523. https://doi.org/10.1038/nrn3084.

9. Poulet, J.F.A., and Crochet, S. (2019). The cortical states of wakefulness. Front. Syst. Neurosci. *12*, 1–18. https://doi.org/10.3389/fnsys.2018.00064.

10. Cole, N., Harvey, M., Myers-Joseph, D., Gilra, A., and Khan, A.G. (2024). Prediction-error signals in anterior cingulate cortex drive task-switching. Nat. Commun. *15*. https://doi.org/10.1038/s41467-024-51368-9.

11. Poulet, J.F.A., and Petersen, C.C.H. (2008). Internal brain state regulates membrane potential synchrony in barrel cortex of behaving mice. Nature *454*, 881–885. https://doi.org/10.1038/nature07150.

12. Crochet, S., and Petersen, C.C.H. (2006). Correlating whisker behavior with membrane potential in barrel cortex of awake mice. Nat. Neurosci. *9*, 608–610. https://doi.org/10.1038/nn1690.

13. Greenberg, D.S., Houweling, A.R., and Kerr, J.N.D. (2008). Population imaging of ongoing neuronal activity in the visual cortex of awake rats. Nat. Neurosci. *11*, 749–751. https://doi.org/10.1038/nn.2140.

14. Adamantidis, A.R., Gutierrez Herrera, C., and Gent, T.C. (2019). Oscillating circuitries in the sleeping brain. Nat. Rev. Neurosci. *20*, 746–762. https://doi.org/10.1038/s41583-019-0223-4.

15. Sanchez-Vives, M. V. (2020). Origin and dynamics of cortical slow oscillations. Curr. Opin. Physiol. *15*, 217–223. https://doi.org/10.1016/j.cophys.2020.04.005.

16. Neske, G.T. (2016). The slow oscillation in cortical and thalamic networks: Mechanisms and functions. Front. Neural Circuits *9*, 1–25. https://doi.org/10.3389/fncir.2015.00088.

17. Staresina, B.P., Bergmann, T.O., Bonnefond, M., Van Der Meij, R., Jensen, O., Deuker, L., Elger, C.E., Axmacher, N., and Fell, J. (2015). Hierarchical nesting of slow oscillations, spindles and

ripples in the human hippocampus during sleep. Nat. Neurosci. *18*, 1679–1686. https://doi.org/10.1038/nn.4119.

18. Steriade, M., Nuñez, A., and Amzica, F. (1993). A novel slow (<1 Hz) oscillation of neocortical neurons in vivo: Depolarizing and hyperpolarizing components. J. Neurosci. *13*, 3252–3265. https://doi.org/10.1523/jneurosci.13-08-03252.1993.

19. Steriade, M., Nuñez, A., and Amzica, F. (1993). Intracellular analysis of relations between the slow (<1 Hz) neocortical oscillation and other sleep rhythms of the electroencephalogram. J. Neurosci. *13*, 3266–3283. https://doi.org/10.1523/jneurosci.13-08-03266.1993.

20. Maria V. Sanchez-Vives, and David A. McCormick (2000). Cellular and network mechanisms of rhythmic recurrent activity in neocortex Maria. Nat. Neurosci. *3*, 1027–1034.

21. Timofeev, I., Grenier, F., Bazhenov, M., Sejnowski, T.J., and Steriade, M. (2000). Origin of slow cortical oscillations in deafferented cortical slabs. Cereb. Cortex *10*, 1185–1199. https://doi.org/10.1093/cercor/10.12.1185.

22. David, F., Schmiedt, J.T., Taylor, H.L., Orban, G., Di Giovanni, G., Uebele, V.N., Renger, J.J., Lambert, R.C., Leresche, N., and Crunelli, V. (2013). Essential thalamic contribution to slow waves of natural sleep. J. Neurosci. *33*, 19599–19610. https://doi.org/10.1523/JNEUROSCI.3169-13.2013.

23. Rigas, P., and Castro-Alamancos, M.A. (2007). Thalamocortical up states: Differential effects of intrinsic and extrinsic cortical inputs on persistent activity. J. Neurosci. *27*, 4261–4272. https://doi.org/10.1523/JNEUROSCI.0003-07.2007.

24. Lemieux, M., Chen, J.Y., Lonjers, P., Bazhenov, M., and Timofeev, I. (2014). The impact of cortical deafferentation on the neocortical slow oscillation. J. Neurosci. *34*, 5689–5703. https://doi.org/10.1523/JNEUROSCI.1156-13.2014.

25. Contreras, D., and Steriade, M. (1995). Cellular Basis of EEG Slow Rhythms: A Study of Dynamic Corticothalamic Relationships. J. Neurosci. *15*, 604–622. https://doi.org/10.1523/jneurosci.15-01-00604.1995.

26. Hasenstaub, A., Sachdev, R.N.S., and McCormick, D.A. (2007). State changes rapidly modulate cortical neuronal responsiveness. J. Neurosci. *27*, 9607–9622. https://doi.org/10.1523/JNEUROSCI.2184-07.2007.

27. Ji, D., and Wilson, M.A. (2007). Coordinated memory replay in the visual cortex and hippocampus during sleep. Nat. Neurosci. *10*, 100–107. https://doi.org/10.1038/nn1825.

28. Petersen, C.C.H., Hahn, T.T.G., Mehta, M., Grinvald, A., and Sakmann, B. (2003). Interaction of sensory responses with spontaneous depolarization in layer 2/3 barrel cortex. Proc. Natl. Acad. Sci. U. S. A. *100*, 13638–13643. https://doi.org/10.1073/pnas.2235811100.

29. Durán, E., Yang, M., Neves, R., Logothetis, N.K., and Eschenko, O. (2021). Modulation of Prefrontal Cortex Slow Oscillations by Phasic Activation of the Locus Coeruleus. Neuroscience *453*, 268–279. https://doi.org/10.1016/j.neuroscience.2020.11.028.

30. Gretenkord, S., Rees, A., Whittington, M.A., Gartside, S.E., and Lebeau, F.E.N. (2017). Dorsal vs. ventral differences in fast Up-state-associated oscillations in the medial prefrontal cortex of the urethane-anesthetized rat. J. Neurophysiol. *117*, 1126–1142. https://doi.org/10.1152/jn.00762.2016.

31. Gretenkord, S., Olthof, B.M.J., Stylianou, M., Rees, A., Gartside, S.E., and LeBeau, F.E.N. (2020). Electrical stimulation of the ventral tegmental area evokes sleep-like state transitions under urethane anaesthesia in the rat medial prefrontal cortex via dopamine D1-like receptors. Eur. J. Neurosci. *52*, 2915–2930. https://doi.org/10.1111/ejn.14665.

32. Jercog, D., Roxin, A., Barthó, P., Luczak, A., Compte, A., and De La Rocha, J. (2017). UP-DOWN cortical dynamics reflect state transitions in a bistable network. Elife *6*, 1–33. https://doi.org/10.7554/eLife.22425.

33. Clement, E.A., Richard, A., Thwaites, M., Ailon, J., Peters, S., and Dickson, C.T. (2008). Cyclic and sleep-like spontaneous alternations of brain state under urethane anaesthesia. PLoS One *3*. https://doi.org/10.1371/journal.pone.0002004.

34. Pagliardini, S., Gosgnach, S., and Dickson, C.T. (2013). Spontaneous Sleep-Like Brain State Alternations and Breathing Characteristics in Urethane Anesthetized Mice. PLoS One *8*, 1–10. https://doi.org/10.1371/journal.pone.0070411.

35. Mondino, A., González, J., Li, D., Mateos, D., Osorio, L., Cavelli, M., Castro-Nin, J.P., Serantes, D., Costa, A., Vanini, G., et al. (2024). Urethane anaesthesia exhibits neurophysiological correlates of unconsciousness and is distinct from sleep. Eur. J. Neurosci. *59*, 483–501. https://doi.org/10.1111/ejn.15690.

36. Torao-Angosto, M., Manasanch, A., Mattia, M., and Sanchez-Vives, M. V. (2021). Up and Down States During Slow Oscillations in Slow-Wave Sleep and Different Levels of Anesthesia. Front. Syst. Neurosci. *15*, 1–9. https://doi.org/10.3389/fnsys.2021.609645.

37. Compte, A., Sanchez-Vives, M. V., McCormick, D.A., and Wang, X.J. (2003). Cellular and network mechanisms of slow oscillatory activity (<1 Hz) and wave propagations in a cortical network model. J. Neurophysiol. *89*, 2707–2725. https://doi.org/10.1152/jn.00845.2002.

38. Muller, L., Chavane, F., Reynolds, J., and Sejnowski, T.J. (2018). Cortical travelling waves: Mechanisms and computational principles. Nat. Rev. Neurosci. *19*, 255–268. https://doi.org/10.1038/nrn.2018.20.

39. Jung, F., Stephan, K.E., Backes, H., Moran, R., Gramer, M., Kumagai, T., Graf, R., Endepols, H., and Tittgemeyer, M. (2013). Mismatch Responses in the Awake Rat: Evidence from Epidural Recordings of Auditory Cortical Fields. PLoS One *8*. https://doi.org/10.1371/journal.pone.0063203.

40. Antunes, F.M., Nelken, I., Covey, E., and Malmierca, M.S. (2010). Stimulus-specific adaptation in the auditory thalamus of the anesthetized rat. PLoS One *5*. https://doi.org/10.1371/journal.pone.0014071.

41. Valerio, P., Rechenmann, J., Joshi, S., De Franceschi, G., and Barkat, T.R. (2024). Sequential maturation of stimulus-specific adaptation in the mouse lemniscal auditory system. Sci. Adv. *10*, 1–16. https://doi.org/10.1126/sciadv.adi7624.

42. Stroh, A., Adelsberger, H., Groh, A., Rühlmann, C., Fischer, S., Schierloh, A., Deisseroth, K., and Konnerth, A. (2013). Making Waves: Initiation and Propagation of Corticothalamic Ca2+ Waves In Vivo. Neuron *77*, 1136–1150. https://doi.org/10.1016/j.neuron.2013.01.031.

43. Ruiz-Mejias, M., Ciria-Suarez, L., Mattia, M., and Sanchez-Vives, M. V. (2011). Slow and fast rhythms generated in the cerebral cortex of the anesthetized mouse. J. Neurophysiol. *106*, 2910–2921. https://doi.org/10.1152/jn.00440.2011.

44. Massimini, M., Huber, R., Ferrarelli, F., Hill, S., and Tononi, G. (2004). The sleep slow oscillation as a traveling wave. J. Neurosci. *24*, 6862–6870. https://doi.org/10.1523/JNEUROSCI.1318-04.2004.

45. Lao-Rodríguez, A.B., Przewrocki, K., Pérez-González, D., Alishbayli, A., Yilmaz, E., Malmierca, M.S., and Englitz, B. (2023). Neuronal responses to omitted tones in the auditory brain: A neuronal correlate for predictive coding. Sci. Adv. https://doi.org/10.1126/sciadv.abq8657.

46. Awwad, B., Jankowski, M.M., Polterovich, A., Bashari, S., and Nelken, I. (2023). Extensive representation of sensory deviance in the responses to auditory gaps in unanesthetized rats. Curr. Biol. *33*, 3024-3030.e3. https://doi.org/10.1016/j.cub.2023.06.013.

47. Auksztulewicz, R., Rajendran, V.G., Peng, F., Schnupp, J.W.H., and Harper, N.S. (2023). Omission responses in local field potentials in rat auditory cortex. BMC Biol. *21*, 1–16. https://doi.org/10.1186/s12915-023-01592-4.

48. Keller, G.B., and Mrsic-Flogel, T.D. (2018). Predictive Processing: A Canonical Cortical Computation. Neuron *100*, 424–435. https://doi.org/10.1016/j.neuron.2018.10.003.

49. Yaron, A., Shiramatsu-Isoguchi, T., Kern, F.B., Ohki, K., Takahashi, H., and Chao, Z.C. (2025). Auditory cortex neurons that encode negative prediction errors respond to omissions of sounds in a predictable sequence. PLOS Biol. *23*, 1–30. https://doi.org/10.1371/journal.pbio.3003242.

50. O'Toole, S.M., Oyibo, H.K., and Keller, G.B. (2023). Molecularly targetable cell types in mouse visual cortex have distinguishable prediction error responses. Neuron *111*, 2918-2928.e8. https://doi.org/10.1016/j.neuron.2023.08.015.

51. Loewy, D.H., Campbell, K.B., De Lugt, D.R., Elton, M., and Kok, A. (2000). The mismatch negativity during natural sleep: Intensity deviants. Clin. Neurophysiol. *111*, 863–872. https://doi.org/10.1016/S1388-2457(00)00256-X.

52. Casado-Román, L., Carbajal, G. V., Pérez-González, D., and Malmierca, M.S. (2020). Prediction error signaling explains neuronal mismatch responses in the medial prefrontal cortex. PLoS Biol. *18*, 1–29. https://doi.org/10.1371/journal.pbio.3001019.

53. Xiong, Y. (Sophy), Donoghue, J.A., Lundqvist, M., Mahnke, M., Major, A.J., Brown, E.N., Miller, E.K., and Bastos, A.M. (2024). Propofol- mediated loss of consciousness disrupts predictive routing and local field phase modulation of neural activity. Proc. Natl. Acad. Sci. *121*. https://doi.org/10.1073/pnas.

54. O'Brien, J.H. (1982). P300 wave elicited by a stimulus-change paradigm in acutely prepared rats. Physiol. Behav. *28*, 711–713. https://doi.org/10.1016/0031-9384(82)90056-7.

55. Tóth, A., Traub, M., Bencsik, N., Détári, L., Hajnik, T., and Dobolyi, A. (2024). Sleep- and sleep deprivation-related changes of vertex auditory evoked potentials during the estrus cycle in female rats. Sci. Rep. *14*, 1–18. https://doi.org/10.1038/s41598-024-56392-9.

56. Hockley, A., and Malmierca, M.S. (2024). Auditory processing control by the medial prefrontal cortex : A review of the rodent functional organisation. Hear. Res. *443*, 108954. https://doi.org/10.1016/j.heares.2024.108954.

57. Sterzer, P., Adams, R.A., Fletcher, P., Frith, C., Lawrie, S.M., Muckli, L., Petrovic, P., Uhlhaas, P., Voss, M., and Corlett, P.R. (2018). The Predictive Coding Account of Psychosis. Biol. Psychiatry *84*, 634–643. https://doi.org/10.1016/j.biopsych.2018.05.015.

58. Sapey-Triomphe, L.A., Pattyn, L., Weilnhammer, V., Sterzer, P., and Wagemans, J. (2023). Neural correlates of hierarchical predictive processes in autistic adults. Nat. Commun. *14*. https://doi.org/10.1038/s41467-023-38580-9.

59. Kocagoncu, E., Klimovich-Gray, A., Hughes, L.E., and Rowe, J.B. (2021). Evidence and implications of abnormal predictive coding in dementia. Brain *144*, 3311–3321. https://doi.org/10.1093/brain/awab254.

60. Lee, M., Sehatpour, P., Hoptman, M.J., Lakatos, P., Dias, E.C., Kantrowitz, J.T., Martinez, A.M., and Javitt, D.C. (2017). Neural mechanisms of mismatch negativity dysfunction in schizophrenia. Mol. Psychiatry *22*, 1585–1593. https://doi.org/10.1038/mp.2017.3.

61. Ross, J.M., and Hamm, J.P. (2024). An expanding repertoire of circuit mechanisms for visual prediction errors. Trends Neurosci. *xx*, 1–2. https://doi.org/10.1016/j.tins.2024.10.007.

62. Garrido, M.I., Kilner, J.M., Stephan, K.E., and Friston, K.J. (2009). The mismatch negativity: A review of underlying mechanisms. Clin. Neurophysiol. *120*, 453–463. https://doi.org/10.1016/j.clinph.2008.11.029.

63. Malmierca, M.S., Carbajal, G. V., and Escera, C. (2019). Deviance Detection and Encoding Acoustic Regularity in the Auditory Midbrain https://doi.org/10.1093/oxfordhb/9780190849061.013.19.

64. Fitzgerald, K., and Todd, J. (2020). Making Sense of Mismatch Negativity. Front. Psychiatry *11*, 1–19. https://doi.org/10.3389/fpsyt.2020.00468.

65. Strauss, M., Sitt, J.D., King, J.R., Elbaz, M., Azizi, L., Buiatti, M., Naccache, L., Van Wassenhove, V., and Dehaene, S. (2015). Disruption of hierarchical predictive coding during sleep. Proc. Natl.

Acad. Sci. U. S. A. *112*, E1353–E1362. https://doi.org/10.1073/pnas.1501026112.

66. Nashida, T., Yabe, H., Sato, Y., Hiruma, T., Sutoh, T., Shinozaki, N., and Kaneko, S. (2000). Automatic auditory information processing in sleep. Sleep *23*, 821–828. https://doi.org/10.1093/sleep/23.6.1i.

67. Sallinen, M., Kaartinen, J., and Lyytinen, H. (1994). Is the appearance of mismatch negativity during stage 2 sleep related to the elicitation of K-complex? Electroencephalogr. Clin. Neurophysiol. *91*, 140–148. https://doi.org/10.1016/0013-4694(94)90035-3.

68. Quaedflieg, C.W., Münte, S., Kalso, E., and Sambeth, A. (2014). Effects of remifentanil on processing of auditory stimuli: A combined MEG/EEG study. J. Psychopharmacol. *28*, 39–48. https://doi.org/10.1177/0269881113512036.

69. Koelsch, S., Heinke, W., Sammler, D., and Olthoff, D. (2006). Auditory processing during deep propofol sedation and recovery from unconsciousness. Clin. Neurophysiol. *117*, 1746–1759. https://doi.org/10.1016/j.clinph.2006.05.009.

70. Malmierca, M.S., Cristaudo, S., Pérez-González, D., and Covey, E. (2009). Stimulus-specific adaptation in the inferior colliculus of the anesthetized rat. J. Neurosci. *29*, 5483–5493. https://doi.org/10.1523/JNEUROSCI.4153-08.2009.

71. Ayala, Y.A., and Malmierca, M.S. (2015). Cholinergic modulation of stimulus-specific adaptation in the inferior colliculus. J. Neurosci. *35*, 12261–12272. https://doi.org/10.1523/JNEUROSCI.0909-15.2015.

72. Taaseh, N., Yaron, A., and Nelken, I. (2011). Stimulus-specific adaptation and deviance detection in the rat auditory cortex. PLoS One *6*. https://doi.org/10.1371/journal.pone.0023369.

73. Polterovich, A., Jankowski, M.M., and Nelken, I. (2018). Deviance sensitivity in the auditory cortex of freely moving rats. PLoS One *13*, 3–8. https://doi.org/10.1371/journal.pone.0197678.

74. Polich, J. (2003). Theoretical Overview of P3a and P3b. Detect. Chang., 83–98. https://doi.org/10.1007/978-1-4615-0294-4_5.

75. Polich, J., and Kok, A. (1995). Cognitive and biological determinants of P300: an integrative review. Biol. Psychol. *41*, 103–146. https://doi.org/10.1016/0301-0511(95)05130-9.

76. Verleger, R. (2020). Effects of relevance and response frequency on P3b amplitudes: Review of findings and comparison of hypotheses about the process reflected by P3b. Psychophysiology *57*, 1–22. https://doi.org/10.1111/psyp.13542.

77. Dasilva, M., Camassa, A., Navarro-Guzman, A., Pazienti, A., Perez-Mendez, L., Zamora-López, G., Mattia, M., and Sanchez-Vives, M. V. (2021). Modulation of cortical slow oscillations and complexity across anesthesia levels. Neuroimage *224*, 117415. https://doi.org/10.1016/j.neuroimage.2020.117415.

78. Möhring, L., and Gläscher, J. (2023). Prediction errors drive dynamic changes in neural patterns that guide behavior. Cell Rep. *42*. https://doi.org/10.1016/j.celrep.2023.112931.

79. Den Ouden, H.E.M., Daunizeau, J., Roiser, J., Friston, K.J., and Stephan, K.E. (2010). Striatal prediction error modulates cortical coupling. J. Neurosci. *30*, 3210–3219. https://doi.org/10.1523/JNEUROSCI.4458-09.2010.

80. Escera, C., Yago, E., Corral, M.J., Corbera, S., and Nuñez, M.I. (2003). Attention capture by auditory significant stimuli: Semantic analysis follows attention switching. Eur. J. Neurosci. *18*, 2408–2412. https://doi.org/10.1046/j.1460-9568.2003.02937.x.

81. Escera, C. (1990). Neural Mechanisms of Involuntary Attention to Acoustic Novelty and Change. J. Cogn. Neurosci. *10*, 590–604.

82. Benusiglio, D., and Asari, H. (2024). Sudden sensory events trigger modality- independent responses across layers in the mouse neocortex.

83. Hockley, A., Bohórquez, L.H., and Malmierca, M.S. (2025). Top-down prediction signals from the medial prefrontal cortex govern auditory cortex prediction errors. Cell Rep. *44*. https://doi.org/10.1016/j.celrep.2025.115538.

84. Berger, J.I., Owen, W., Wilson, C.A., Hockley, A., Coomber, B., Palmer, A.R., and Wallace, M.N. (2018). Gap-induced reductions of evoked potentials in the auditory cortex: A possible objective marker for the presence of tinnitus in animals. Brain Res. *1679*. https://doi.org/10.1016/j.brainres.2017.11.026.

578 **STAR★METHODS**

579 **KEY RESOURCES TABLE**

580

REAGENT or RESOURCE	SOURCE	IDENTIFIER
Chemicals, peptides, and recombinant proteins		
Urethane	Merk	CAT#U2500-100; CAS: 51-79-6
Ketamine (Ketamidor)	Veternova/Ritcher Pharma	C.N: 580393.7
Xylazine (Rompun)	Veternova/Bayer	C.N: 572126.2
Lidocaine	B. Braun	C.N: 645598.2
Atropine	B. Braun	C.N: 635649.4
Dexametaxona (Cortexonavet)	Veternova/Syva	C.N: 585299.7
Meloxicam (Metacam)	Veternova/Boehringer Ingelheim	C.N: 570971.0
Buprenorphine (Bupaq)	Veternova/Ritcher Pharma	C.N: 578816.6
Tri-antibiotic (Dermisone)	Novartis	C.N: 952986
Betadine	MEDA	C.N: 694109.6
KwikCast	World Precision Instruments	CAT#KWIK-CAST
Duralay Dental cement	Reliance	2244
Experimental models: Organisms/strains		
RjOrl:LE (Long Evans)	Janvier Labs	CAT#LONG EVANS rat
Software and algorithms		
BioSigRZ ABR	Tucker-Davis Technologies, Inc	https://www.tdt.com/component/biosigrz-abr-dpoae-software/
MATLAB 2024a	MathWorks	https://es.mathworks.com/products/matlab.html
Original data analysis code	This study	10.5281/zenodo.15791285
Original data	This study	10.5281/zenodo.15791248
Other		
RZ6 MULTI-I/O Processor	Tucker-Davis Technologies, Inc	CAT#RZ6
Medusa4Z ABR Amplifier	Tucker-Davis Technologies, Inc	CAT#Medusa4Z
PZ5 Flexible Amplifiers	Tucker-Davis Technologies, Inc	CAT#PZ5
RZ2 BioAmp Processor	Tucker-Davis Technologies, Inc	CAT#RZ2
RZ5 BioAmp Processor	Tucker-Davis Technologies, Inc	CAT#RZ5
RA16PA 1S Channel Medusa Preamp	Tucker-Davis Technologies, Inc	CAT#RA16PA

ZCA-EIB16 ZIF-Clip® Headstage to Electrode Interface Board (16 Channels)	Tucker-Davis Technologies, Inc	CAT# ZCA-EIB16
Wire silver Tef 0.125mm 10Ft	World Precision Instruments, Inc.	CAT#AGT0510

EXPERIMENTAL MODEL AND STUDY PARTICIPANT DETAILS

All animal experimental procedures were performed under protocols established by the Directive of the European Communities (86/609/CEE, 2003/65/CE, and 2010/63/UE) and RD53/2013 Spanish Legislation for the use and care of animals. All the details of the study were approved by the Bioethics Committee of the University of Salamanca (USAL-ID-887). Seven Female Long-Evans rats were obtained from Janvier Labs (Le Genest-Saint-Isle, France), and experiments were performed on animals weighing 210-280g. Rats were housed on a 12/12 h light-dark cycle, with food and water available *ad libitum*.

METHOD DETAILS

Anesthetic induction and auditory brainstem responses

All experiments were made inside a chamber with acoustic insulation and electrical protection. For acute experiments, anesthesia was induced with urethane (1.9 g kg^{-1}, i.p.; Sigma-Aldrich, St Louis, U.S.A.), then a further 0.315 - 0.63 g kg^{-1} dose at 45 minutes if required to induce surgical anesthetic depth. This dose is greater than that used previously to induce robust synchronised states consisting of Up and Down states [29]. For chronic implant anesthesia was induced with ketamine (Ketamidor, 50 mg kg^{-1}, i.p.; Richter Pharma, Wels, Austria) and xylazine (Rompun, 5 mg kg^{-1}, i.p.; Bayer, Berlin, Germany) and recovery protocol was followed as previously [83]. Corneal and rear paw withdrawal reflexes were routinely monitored. Ophthalmic gel (Lipolasic 2 mg/g; Bausch Lomb, Vaughan, Canada) was applied for avoid dry eyes in the animals. During all experimental procedures, the animals were artificially ventilated through a tracheotomy with O_2, monitoring the CO_2 levels; except for the chronic implanted animal, where no tracheostomy was performed. Temperature was maintained at 36 - 38°C using a rectal probe and a homeostatic heating blanket (Cibertec, Madrid, Spain) placed under the animal.

Sound stimuli were presented using Tucker-Davis Technologies (TDT; Alachua, FL, USA) hardware and presented monaurally to the right ear through a closed system using a custom-made earphone (calibrated to ensure a flat spectrum; ±2 dB at 0.5 - 44 kHz) coupled to a custom-made cone, as a substitute for traditional ear bars. Initially, auditory brainstem responses (ABRs) were recorded to check for normal hearing in animals. Three needle electrodes were placed into the skin, one at the dorsal midline close to the neural crest, one behind the left pinna, and one behind the right pinna. ABRs were recorded in response to tone bursts (4, 8, 16 and 32 kHz; 5 ms duration, 1 ms rise/fall times, 21 Hz presentation rate, 512 repetitions in 10 dB steps from 0–80 dB SPL; Tucker-Davis Technologies RZ6 & Medusa 4Z preamp). ABR thresholds were analysed with TDT BioSigRZ and all animals showed thresholds ≤40 dB SPL and were considered normal hearing for the following experiments.

Surgery and ECoG array implantation

Following ABRs, dexamethasone (Cortexonavet, 0.25 mg kg−1, i.m.; Syva, León, Spain) and atropine (0.1 mg kg−1, s.c.; Braun, Rubi, Spain) were administered to reduce cerebral oedema and bronchial secretions, respectively. Lidocaine was also injected around the pinna tissue to achieve a higher anaesthetic level in these areas. The ears were prepared by removing pinna cartilage to obtain easier access the ear canal, and a tracheotomy allowed artificial ventilation. The animal was placed in the stereotactic frame with the upper jaw attached to a bite bar and the hollow ear bars into the ear canals. The speaker was placed into the right ear bar, while the hollow left ear bar was filled with plasticine. A midline incision was made along the midline of the head, from 5 mm rostral of bregma to the nuchal ridge, as well as small lateral incisions (~3 mm) at each end. Connective tissue was removed and the temporalis muscle moved to allow access to AC-L, AC-R, mPFC-L and mPFC-R. An electrode array was produced, made of 8 silver wires (0.125 mm diameter; WPI, Sarasota, USA) heated at one end to form a ball, to prevent damage to the dura mater, and attached to a ZCA-EIB16 (TDT, Alachua, USA) ZIF-clip

connector board [84]. A total of 10 burr holes were drilled for electrode placement and anchor screws, at the locations shown in Fig 1A. Silver ball electrodes were placed in the burr holes on the rostral and caudal AC and mPFC. After electrode insertion, the drill holes were filled with Kwik-Cast silicone sealant (World Precision Instruments, Hitchin, UK) and then the entire array covered with dental acrylic (Duralay; Reliance Dental Manufacturin; Alsip, IL, USA). Finally, skin was sutured around the implant. 6 Animals were not allowed to recover, and first recordings were made approximately 1 hour after the end of the surgery. One rat was chronically implanted, after the surgery, the animal was treated during the following 3-5 days until the disappearance of the symptoms. This included the administration of anti-inflammatory every 24h (Metacam, 1 mg kg^{-1}, s.c.; Boehringer Ingelheim, Ingelheim am Rhein, Germany), analgesic every 12h (Bupaq 0.1 mg kg^{-1}, s.c.; Richter Pharma AG, Wels, Austria) and a topical triantibiotic every 24h (Dermisone; Novartis, Basilea, Switzerland).

Neural recording and analysis

Custom MATLAB (Mathworks, Natick, USA) code was used to generate stimuli patterns and control presentation through TDT Synapse software. Stimuli were output from the TDT RZ6 and presented through a speaker to the right ear. A TDT ZC16 headstage was used to connect the implanted electrodes to a TDT PZ5 preamp connected to a TDT RZ2 processor. The data were filtered (low-pass 7 kHz) and recorded using TDT Synapse software at a sampling rate of 3 kHz. We analysed the TDT stream data as LFP data using custom Matlab scripts. The stream was downsampled to 763 Hz, then filtered using an 8th order bandpass filter (0.1-10 Hz for LFPs; 0.1-150 Hz for oscillation analysis). Oscillatory analysis bands used were: delta, 2-4 Hz; theta 4-8 Hz; alpha 8-14 Hz; beta 14-30 Hz; low gamma 30-70 Hz; high gamma 70-150 Hz.

QUANTIFICATION AND STATISTICAL ANALYSIS

Up state initiation found in LFP traces using the Matlab findpeaks function (MinPeakDistance = 382; MinPeakProminence = 3 standard deviations). Peaks that had another peak in the preceding 1.5s were removed, as they were later waves of the same Up state. All further analysis, statistical testing and plotting of all data were performed using custom MATLAB scripts. Cross-correlation synchrony was calculated using a bin size of 50 ms. Total synchrony was quantified as the total synchrony measurement for a 250 ms window centered at the peak synchrony timing. Synchrony measures for were statistically compared using two-sample t-tests, comparing the synchrony of the DEV-Up to the synchrony of the STD-Up for the standards preceding the DEV by 2-5 trials.